RNA

PANC-1 cells (70×10^4/well) were plated in a DMEM medium supplemented with 2% FBS treated with dextran-coated charcoal (DCC). The next day, the cells were cultured in the absence or presence of 10 ng/mL recombinant human transforming growth factor (TGF)-β1 (R&D Systems, Mineapolis, MN, USA) in the DMEM medium supplemented with 2% DCC-treated FBS. After a 48 h incubation, total cellular RNA were prepared from the cells using a TRIzol reagent (Invitrogen, Carlsbad, CA, USA).

Real-time polymerase chain reaction

The nine aforementioned cDNA samples were cycled for PCR by an ABI PRISM 7700 (Applied Biosystems, Foster City, CA, USA), monitoring the signals from TaqMan probes. Primer sets used were: human claudin-1 forward primer, 5′-TACTCCTATGCCGGCGACA-3′; reverse primer, 5′-GACATCCACAGCCCCTCGT-3′; TaqMan primer, Fam-CGTGACCGCCCAGGCCATG-Tamra; human claudin-4 forward primer, 5′-CATCGGCAGCAACATTGTCA-3′; reverse primer, 5′-GCACCTTACACGTAGTTGCT-3′; TaqMan primer, Fam-TGGTGCAGAGCACCGGCCA-Tamra; human β-actin forward primer; 5′-TGAGCGCGGCTACAGCTT-3′; reverse primer, 5′-TCCTTAATGTCACGCACG-3′; and TaqMan primer, Fam-ACCACCACGGCCGAGCGG-Tamra.

Statistics

Data were statistically analyzed using Statcel software (OMS, Tokyo, Japan).

RESULTS

Immunohistochemistry findings

In human adult pancreatic tissues, both claudin-1 and claudin-4 had clear membrane immunostainings in acinar cells (Fig. 1a,b). Positive immunostainings for claudin-1 and claudin-4 were also found in branching pancreatic ducts and terminal ductules, but the intensity was weaker than that of acinar cells (Fig. 1a,b and data not shown). The signals for claudin-1 and claudin-4 were absent in islet cells (data not shown). In addition, positive immunostainings for claudin-1 and claudin-4 were also found in the main pancreatic duct of the ampulla region, although the expression patterns were somewhat different from each other. The claudin-1-positive cells were mainly found in the glandular cells, while the claudin-4-positive cells were found mainly in the surface epithelial cells (Fig. 1c,d).

Of 12 cases of ductal adenocarcinomas, 11 (92%) were positive for claudin-4 and seven (58%) for claudin-1 (Fig. 1e,f; Table 2). Although claudin-4 had clear and membranous stainings in most cases, and despite the rather weak stainings of claudin-1, there was no statistical significance between claudin-1 and claudin-4 expressions by Mann–Whitney *U*-test.

Of 17 IPMT adenoma lesions, 14 (82%) were positive for claudin-1, while four (24%) were positive for claudin-4 (Fig. 2a–c; Table 2). In contrast with the adenoma data, out of six non-invasive carcinoma lesions, three (50%) were positive for claudin-1, and five (83%) were positive for claudin-4 (Fig. 2g–i; Table 2). In invasive carcinoma lesions, one out of five (20%) was positive for claudin-1, and four (80%) were positive for claudin-4. There was no stastical difference of the immunostainings between non-invasive and invasive carcinomas. In addition, three out of 10 borderline lesions (30%) were positive for claudin-1, and five (50%) were positive for claudin-4, three out of six hyperplastic foci (50%) were positive for claudin-1, and none was positive for claudin-4 (Fig. 2d–f; Table 2). The immunostaining pattern of claudin-4 had a statistically positive correlation, while that of claudin-1 had a negative correlation between the immunostaining pattern and the histological tumor grades by the Spearman correlation coefficient rank test.

The immunohistochemical data of the 38 IPMT lesions excepting six hyperplastic foci were re-analyzed according to the subtypes. Nine out of 10 lesions (90%) in clear-cell types were positive for claudin-1, while two (20%) were positive for claudin-4 (Fig. 2a–c; Table 3). In contrast, seven out of 20

Table 2 Claudin-1 and claudin-4 in ductal adenocarcinomas and IPMT

	Claudin-1 immunoreactivity						Claudin-4 immunoreactivity					
	Total	−	±	+	++	Positive (%)	Total	−	±	+	++	Positive (%)
Ductal adenocarcinoma	12	2	3	5	2	58	12	1	0	6	5	92
IPMT												
Hyperplasia	6	1	2	1	2	50	6	4	2	0	0	0
Adenoma	17	1	2	5	9	82	17	10	3	4	0	24
Borderline	10	2	5	3	0	30	10	2	3	3	2	50
Carcinoma	6	0	4	2	0	33	6	0	1	1	4	83
Invasive carcinoma	5	2	2	1	0	20	5	0	1	2	2	80

IPMT, intraductal papillary–mucinous tumor.

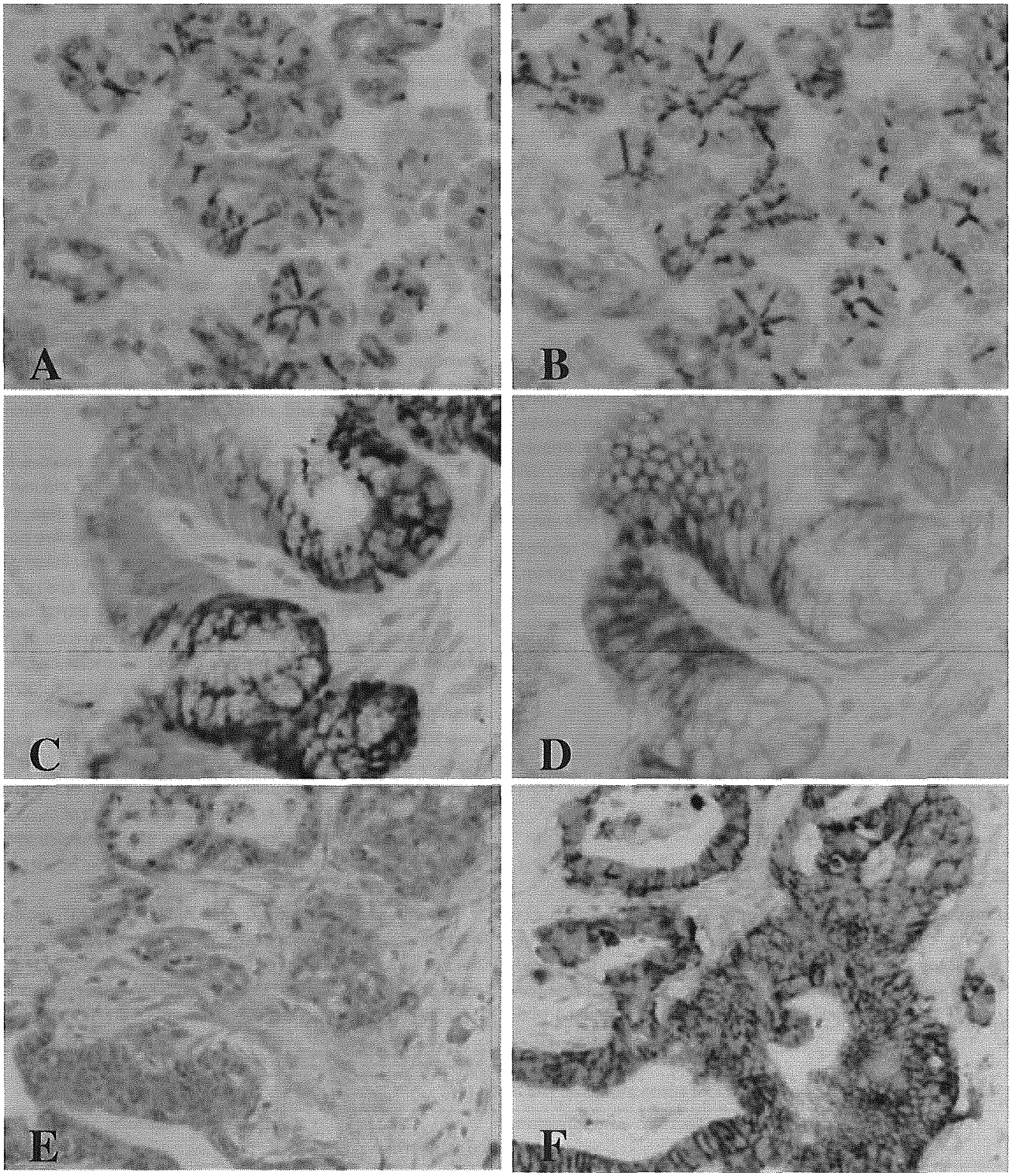

Figure 1 Claudin-1 and claudin-4 immunostainings in human adult pancreatic tissues and pancreatic ductal carcinomas. (**A,B**) Claudin-1 and claudin-4 immunostainings in the peripheral pancreatic tissue. Membranous immunostainings were distinctly found in acinar cells, and weakly in ductal epithelia of human adult pancreatic tissues (**A**, claudin-1; **B**: claudin-4). (**C,D**) Claudin-1 and claudin-4 immunostainings in the main pancreatic duct. In the main pancreatic duct, the immunostaining of claudin-4 was mainly found in the surface epithelia, while that of claudin-1 was in the glandular portions (**C**, claudin-1; **D**, claudin-4). (**E,F**) Claudin-1 and claudin-4 immunostainings in the pancreatic ductal adenocarcinoma. Membranous immunostaining was marked in ductal adenocarcinoma cells for claudin-4, but less for claudin-1 (**E**, claudin-1; **F**, claudin-4).

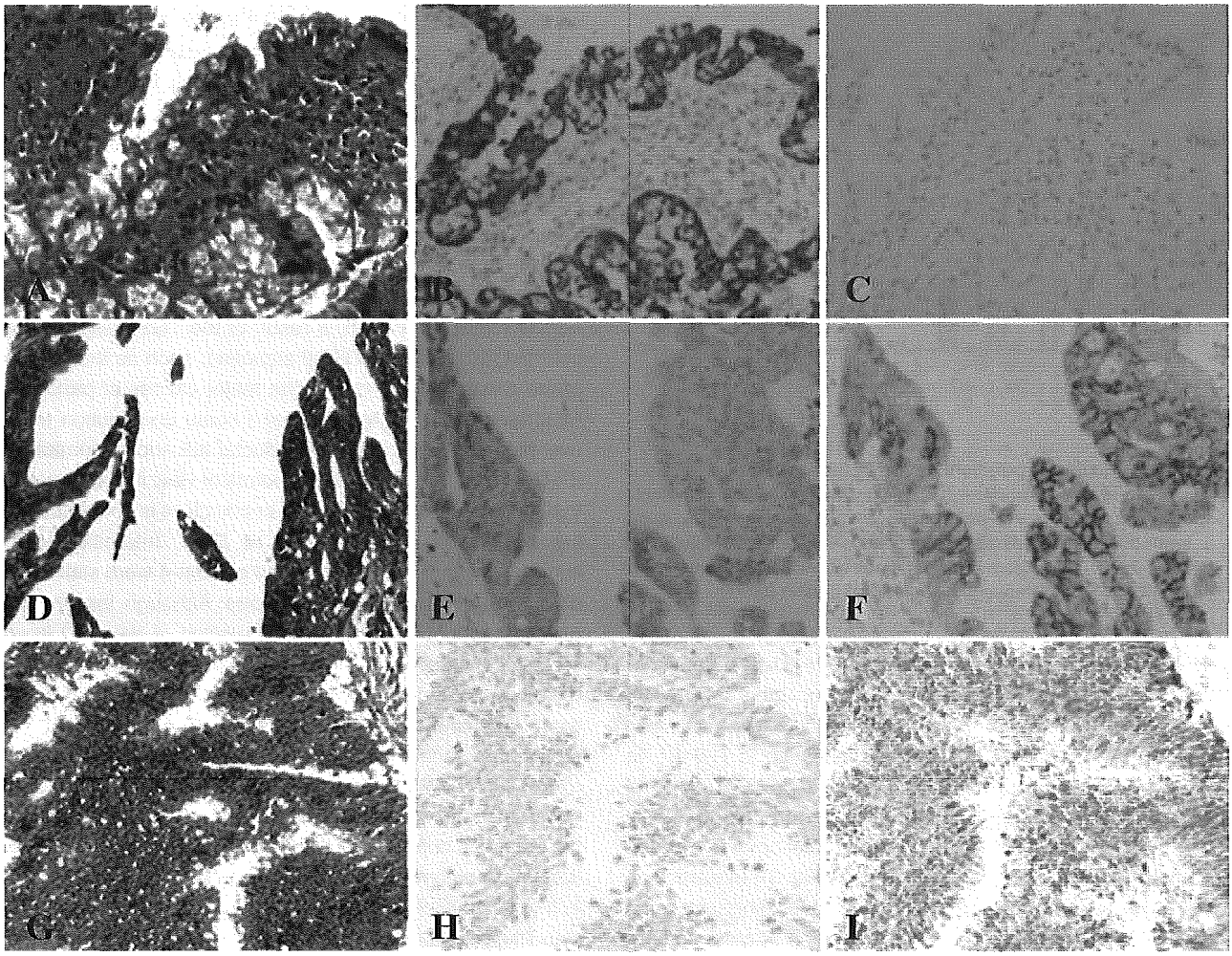

Figure 2 Claudin-1 and claudin-4 immunostainings in intraductal papillary and mucinous tumors (IPMT). (**A–C**) Claudin-1 and claudin-4 immunostainings in the clear-cell type of IPMT adenoma. The immunostaining of claudin-1 was marked, but that of claudin-4 was completely absent (**A**, HE; **B**, claudin-1; **C**, claudin-4). (**D–F**) Claudin-1 and claudin-4 immunostainings in the compact-cell type of borderline tumor. Claudin-1 showed focal and cytoplasmic immunostaining, while claudin-4 showed clear membranous immunostaining mainly in the claudin-1-negative cells (**D**, HE; **E**, claudin-1; **F**, claudin-4). (**G–I**) Immunostainings of claudin-1 and claudin-4 in the dark-cell type of IPMT carcinoma. Immunostaining of claudin-4 was marked in the lateral membranes of most carcinoma cells, but that of claudin-1 was absent in the lateral membranes (**G**, HE; **H**, claudin-1; **I**, claudin-4).

Table 3 Claudin-1 and claudin-4 in the subtypes of IPMT

		Claudin-1 immunoreactivity				Claudin-4 immunoreactivity			
	Total	–	±	+	++	–	±	+	++
Clear	10	0	1	2	7	7	1	2	0
Dark	20	3	10	6	1	4	3	5	8
Compact	8	2	2	3	1	1	4	3	0

IPMT, intraductal papillary–mucinous tumor.

lesions (35%) in dark-cell types were positive for claudin-1, while 13 (65%) were positive for claudin-4 (Fig. 2g–i; Table 3). In compact-cell types, four out of eight lesions (50%) were positive for claudin-1, and three (38%) were positive for claudin-4 (Fig. 2d–f; Table 3). The immunohistochemical results of both claudins were statistical different among the IPMT subtypes by Kruskal–Wallis test.

Real-time polymerase chain reaction

We first tested the real-time PCR conditions using human pancreatic cancer PANC-1 cells. The transcriptional level of claudin-4 was prominent in PANC-1 cells, reaching up to 8.4×10^5 fmol/pmol. Concordant with a previous report,[7] the transcriptional level of claudin-4 was drastically decreased, to 0.2% of the unstimulated level, when PANC-1 cells were

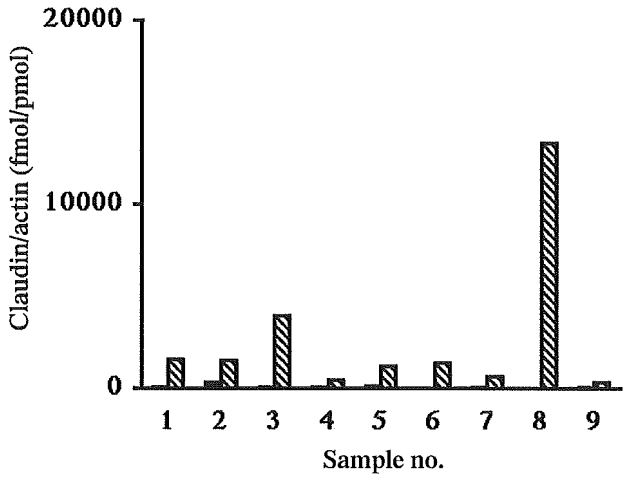

Figure 3 Real-time polymerase chain reaction (PCR) analysis of claudin-1 (■) and claudin-4 (▨) in surgically resected pancreatic specimens. Samples 1–3 are from normal pancreatic tissues, 4 and 5 from ductal adenocarcinomas, 6 and 7 from IPMT borderline tumors, and 8 and 9 from IPMT carcinomas. Absolute values (fmol) are adjusted by the transcriptional level of β-actin (pmol).

treated with 10 ng/mL of recombinant TGF-β1. The transcriptional level of claudin-1 was 1.9×10^4 fmol/pmol in PANC-1 cells, much lower than that of claudin-4. Its level was also decreased to 1.8×10^3 fmol/pmol in response to TGF-β1. In surgically resected specimens, the transcriptional levels of claudin-1 and claudin-4 were much lower than those in PANC-1 cells: on the order of 1.0×10^3 fmol/pmol in claudin-4 and 1.0×10^2 fmol/pmol in claudin-1 (Fig. 3). In particular, the lower levels of ductal carcinoma cases suggest some difficulties in sampling because of the rich stromal components in pancreatic ductal adenocarcinomas. Nevertheless, one specimen of IPMT carcinoma expressed a higher level of claudin-4 (Fig. 3).

DISCUSSION

Here we present the distinct expression patterns of claudin-1 and claudin-4 in pancreatic tissues, ductal adenocarcinomas, and IPMT. Both claudin-1 and claudin-4 showed strong membranous immunostainings in acinar cells and mild immunostainings in ductal cells from adult pancreatic tissues. Interestingly, the expression patterns of claudin-1 and claudin-4 were considerably varied in ductal adenocarcinomas and IPMT. In particular, the expression of claudin-1 or claudin-4 was negatively or positively correlated with the histological tumor grades of IPMT. Recent reports have shown that the expression of claudin-1 and claudin-4 is altered under various conditions. For example, an oncogenic *Raf* signal suppresses the expression of claudin-1 in a rat salivary gland epithelial cell line, while the blockade of the *Ras* signal leads to the downregulation of claudin-4 in human pancreatic cancers PANC-1.[7,15] Importantly, it is well known that the *K-ras* mutaion is found in most cases of pancreatic cancers and in considerable cases of IPMT.[16–18] These reported findings allow us to speculate that the dysregulations of claudin-1 and claudin-4 in the present study might be, at least in part, coupled with the activation of the *Ras–Raf* pathway in pancreatic cancers and IPMT carcinomas. In addition, the claudin-4 expression was severely repressed in response to TGF-β in human pancreatic cancer PANC-1 cells. Therefore, it is likely that the downregulation of claudin-4 in IPMT adenomas might be, in part, a result of the TGF-β signaling. In contrast, the deficient TGF-β signaling, such as the deletion of the *Smad 4* gene, one of the major causes of pancreatic tumorigenesis,[19] might also make some contribution to the overexpression of claudin-4 in ductal adenocarcinomas and IPMT carcinomas. From these points of view it seems natural that the expression of claudin-1 or claudin-4 is correlated with the histological tumor grades of IPMT. Interestingly, the immunostainings of claudin-1 and claudin-4 were statistically different among the IPMT subtypes. Although the previous report has mentioned the overexpression of claudin-1 in colorectal cancers,[12] the claudin-1 expression seemed to be higher in IPMT clear-cell types (gastric types) than dark-cell types (intestinal types) in the present study. In addition, our preliminary analysis showed that claudin-4 is strongly expressed in both intestinal and gastric types of gastric adenocarcinomas. Although further studies would be required, the epithelial phenotypes were likely to make some contribution to the preferential expression of claudin-1 and claudin-4 in IPMT. The lack of any statistical significance between the claudin-1 and claudin-4 immunostainings in ductal adenocarcinomas may result from further gene mutations or cellular signaling alterations during tumorigenesis.

Very recently, claudin-4 has been shown to be one of the molecular markers of the invasive phenotypes of IPMT through gene expression profiling.[20] In contrast, it has been also reported that claudin-4 decreases invasiveness and metastatic potential of pancreatic cancers.[7] In addition, other reports have shown that several claudins are involved in cancer progression through the activation of matrix metalloproteinase (MMP)-2.[21,22] To date, the biological significance of the claudin-4 overexpression in pancreatic carcinomas has not been fully understood. Nevertheless, as a receptor of *Clostridium perfringens* enterotoxin (CPE), claudin-4 has become an attractive molecule for a CPE-mediated cytolytic cancer therapy. A number of reports have pointed out the anticancer effects of CPE through claudin-4.[4,23] Although the present real-time PCR failed to demonstrate any correlation between the levels of claudin-1 or claudin-4 and the histological tumor grades, future diagnostic applications for the real-time PCR method will provide useful information about the CPE-mediated therapy.

ACKNOWLEDGMENTS

We would like to thank Dr Sata at Jichi Medical School for his helpful discussions. We also thank M. Mizogami, M. Yanagita, K. Honmou, S. Sato, K. Hidano, M. Kikuchi, M. Hoshino, and Y. Haga for their technical assistance.

REFERENCES

1 Tsukita S, Furuse M, Itoh M. Multifunctional strands in tight junctions. *Nat Rev Mol Cell Biol* 2001; **2**: 285–93.
2 Tsukita S, Furuse M. Claudin-based barrier in simple and stratified cellular sheets. *Curr Opin Cell Biol* 2002; **14**: 531–6.
3 Katoh M, Katoh M. CLDN23 gene, frequently down-regulated in intestinal-type gastric cancer, is a novel member of CLAUDIN gene family. *Int J Mol Med* 2003; **11**: 683–9.
4 Michl P, Buchholz M, Rolke M *et al.* Claudin-4: a new target for pancreatic cancer treatment using *Clostridium perfringens* enterotoxin. *Gastroenterology* 2001; **121**: 678–84.
5 Rangel LBA, Agarwal R, D'Souza T *et al.* Tight junction proteins claudin-3 and claudin-4 are frequently overexpressed in ovarian cancer but not in ovarian cystadenomas. *Clin Cancer Res* 2003; **9**: 2567–75.
6 Long H, Crean CD, Lee W-H, Cummings OW, Gabig TG. Expression of *Clostridium perfringens* enterotoxin receptors claudin-3 and claudin-4 in prostate cancer epithelium. *Cancer Res* 2001; **61**: 7878–81.
7 Michl P, Barth C, Buchholz M *et al.* Claudin-4 expression decreases invasiveness and metastatic potential of pancreatic cancer. *Cancer Res* 2003; **63**: 6265–71.
8 Sessa F, Solicia E, Capella C *et al.* Intraductal papillary-mucinous tumours represent a distinct group of pancreatic neoplasma: an investigation of tumour cell differentiation and K-ras, p53 and c-erbB-2 abnormalities in 26 patients. *Virchows Arch* 1994; **425**: 357–67.
9 Solcia E, Capella C, Klöppel G, eds. *Tumors of the Pancreas.* Washington, DC: Armed Forces Institute of Pathology, 1995.
10 Furuse M, Fujita K, Hiiragi T, Fujimoto K, Tsukita S. Claudin-1 and -2: novel integral membrane proteins localizing at tight junctions with no sequence similarity to occludin. *J Cell Biol* 1998; **141**: 1539–50.
11 Furuse M, Hata M, Furuse K *et al.* Claudin-based tight junctions are crucial for the mammalian epidermal barrier: a lesson from claudin-1-deficient mice. *J Cell Biol* 2002; **156**: 1099–111.
12 Miwa N, Furuse M, Tsukita S, Niikawa N, Nakamura Y, Furukawa Y. Involvement of claudin-1 in the beta-catenin/Tcf signaling pathway and its frequent upregulation in human colorectal cancers. *Oncol Res* 2000; **12**: 469–76.
13 Yonezawa S, Nakamura A, Horinouchi M, Sato E. The expression of several types of mucin is related to the biological behavior of pancreatic neoplasms. *J Hepatobiliary Pancreat Surg* 2002; **9**: 328–41.
14 Fujii A, Kamiakito T, Takayashiki N, Fujii T, Tanaka A. Neuroendocrine tissue-specific transcription factor, BETA2/NeuroD, in gastric carcinomas: a comparison with chromogranin A and synaptophysin expressions. *Pathol Res Prac* 2003; **199**: 513–19.
15 Li D, Mrsny RJ. Oncogenic Raf-1 disrupts epithelial tight junction via downregulation of occludin. *J Cell Biol* 2000; **148**: 791–800.
16 Smit VT, Boot AJ, Smits AM, Fleuren GJ, Cornelisse CJ, Bos JL. KRAS codon 12 mutations occur very frequently in pancreatic adenocarcinomas. *Nucleic Acids Res* 1988; **16**: 7773–82.
17 Griffin CA, Hruban RH, Morsberger LA *et al.* Consistent chromosome abnormalities in adenocarcinoma of the pancreas. *Cancer Res* 1995; **55**: 2394–9.
18 Yoshizawa K, Nagai H, Sakurai S *et al.* Clonality and K-ras mutation analyses of epithelia in intraductal papillary mucinous tumor and mucinous cystic tumor of the pancreas. *Virchows Arch* 2002; **441**: 437–43.
19 Shutte M, Hruban RH, Hedrick L *et al.* DPC4 gene in various tumour types. *Cancer Res* 1996; **56**: 2527–30.
20 Sato N, Fukushima N, Maitra A *et al.* Gene expression profiling identifies genes associated with invasive intraductal papillary mucinous neoplasms of the pancreas. *Am J Pathol* 2004; **164**: 903–14.
21 Miyamori H, Takino T, Kobayashi Y *et al.* Claudin promotes activation of pro-matrix metalloproteinase-2 mediated by membrane-type matrix metalloproteinases. *J Biol Chem* 2001; **276**: 28 204–11.
22 Ellenrieder V, Alber B, Lacher U *et al.* Role of MT-MMPs and MMP-2 in pancreatic cancer progression. *Int J Cancer* 2000; **85**: 14–20.
23 Kominsky SL, Vali M, Korz D *et al. Clostridium perfringens* enterotoxin elicits rapid and specific cytolysis of breast carcinoma cells mediated through tight junction proteins claudin 3 and 4. *Am J Pathol* 2004; **164**: 1627–33.

A Neutralizing Anti–Fibroblast Growth Factor 8 Monoclonal Antibody Shows Potent Antitumor Activity against Androgen-Dependent Mouse Mammary Tumors *In vivo*

Naoki Shimada,[1] Toshihiko Ishii,[2] Teruyoshi Imada,[2] Katsumi Takaba,[2] Yuka Sasaki,[1] Kumiko Maruyama-Takahashi,[1] Yoshimi Maekawa-Tokuda,[2] Hideaki Kusaka,[2] Shiro Akinaga,[2] Akira Tanaka,[3] and Kenya Shitara[1]

Abstract

Purpose: Fibroblast growth factor 8b (FGF8b) has been implicated in oncogenesis of sex hormone–related malignancies. A murine monoclonal anti-FGF8 antibody, KM1334, has been raised against a FGF8b-derived peptide and shown to neutralize FGF8b activity in an androgen-dependent mouse mammary cell line (SC-3) *in vitro* growth. The purpose of this study was to evaluate KM1334 as a therapeutic agent for FGF8-dependent cancer.

Experimental Design: Specificity and neutralizing activity of KM1334 were examined *in vitro*. *In vivo* therapeutic studies were done in nude mice bearing SC-3 tumors s.c.

Results: KM1334 recognized FGF8b and FGF8f specifically out of four human FGF8 isoforms and showed little binding to other members of FGF family. Neutralizing activity of KM1334 was confirmed by both blocking of FGF8b binding to its three receptors (FGFR2IIIc, FGFR3IIIc, and FGFR4) and FGF8b-induced phosphorylation of FGFR substrate 2α and extracellular signal-regulated kinase 1/2 in SC-3 cells. The *in vitro* inhibitory effect could be extended to *in vivo* tumor models, where KM1334 caused rapid regression of established SC-3 tumors in nude mice. This rapid regression of tumors after KM1334 treatment was explained by two independent mechanisms: (*a*) decreased DNA synthesis, as evidenced by a decrease in uptake of 5-bromo-2′-deoxyuridine, and (*b*) induction of apoptosis as shown by the terminal deoxynucleotidyl transferase–mediated nick end labeling assay.

Conclusions: KM1334 possesses strong blocking activity *in vitro* and antitumor activity *in vivo* and therefore may be an effective therapeutic candidate for the treatment of cancers that are dependent on FGF8b signaling for growth and survival.

Since the discovery of monoclonal antibody (mAb) technology (1), attempts have been made to use their exquisite specificity and affinity for the treatment of human diseases, such as cancer. In recent years, significant advances have been made in the therapeutic use of antibodies as shown by the growing numbers that are gaining approval for clinical use (2). Many targets for therapeutic antibodies are membrane-bound antigens, which is necessary for antibodies to show effector functions, such as antibody-dependent cellular cytotoxicity and complement-dependent cytotoxicity. However, soluble molecules, which promote tumor progression directly or indirectly, can also be good targets for cancer therapy. For example, bevacizumab, an anti–vascular endothelial growth factor neutralizing antibody, showed clinical benefits for patients with metastatic colorectal cancer in phase III study (3). For the clinical application of mAbs against growth factors, candidate mAbs having high specificity, potent neutralizing activity, and *in vivo* antitumor activity should be selected for the further development of humanized antibodies.

The fibroblast growth factors (FGF) form a family of at least 24 growth-regulatory proteins. They share 35% to 50% amino acid sequence identity and induce proliferation and differentiation in a wide range of cells of epithelial, mesodermal, and neuroectodermal origin (4, 5). FGF8 was originally isolated from the conditioned medium of an androgen-dependent mouse mammary tumor cell line (SC-3) as an androgen-induced growth factor and was later classified as a member of the FGF family based on structural similarity (6). FGF8 has been found to have an important role in embryogenesis and morphogenesis (7). It is expressed during gastrulation, in brain development, and in the process of limb and facial morphogenesis of the developing mouse (8–13). FGF8 has been identified as an oncogene product based on its transforming activity in NIH3T3 cells (14). In addition, a high frequency of

Authors' Affiliations: [1]Tokyo Research Laboratories, Kyowa Hakko Kogyo Co., Ltd., Tokyo, Japan; [2]Drug Development Research Laboratories Pharmaceutical Research Institute, Kyowa Hakko Kogyo Co., Ltd., Shizuoka, Japan; and [3]Department of Pathology, Jichi Medical School, Tochigi, Japan

Received 11/18/04; revised 2/16/05; accepted 2/17/05.

The costs of publication of this article were defrayed in part by the payment of page charges. This article must therefore be hereby marked *advertisement* in accordance with 18 U.S.C. Section 1734 solely to indicate this fact.

Requests for reprints: Kenya Shitara, Tokyo Research Laboratories, Kyowa Hakko Kogyo, Co., Ltd., 3-6-6 Asahi-machi, Machida, Tokyo 194-8533, Japan. Phone: 81-42-725-0857; Fax: 81-42-725-2689; E-mail: kshitara@kyowa.co.jp.

FGF8 mRNA overexpression, which is associated with decreased patient survival and persists in androgen-independent disease, was detected by tissue *in situ* hybridization in prostate cancer specimens (15).

The structure of the *FGF8* gene is more complicated than that of the other members of the FGF family. Alternative splicing of the *FGF8* gene potentially gives rise to eight different protein isoforms (a-h) in mice and four isoforms (a, b, e, and f) in humans (6, 16, 17). The isoforms differ in the NH_2 terminus. The biological function of these forms is not exactly known, but at least they differ in transforming potential. FGF8b has been found to have the highest NIH3T3 cell-transforming capacity (18, 19). Furthermore, transgenic mice overexpressing FGF8b in the mammary glands are found to develop mammary tumor and those in prostate epithelial cells develop prostatic intraepithelial neoplasia (20, 21). Overexpression of FGF8b gives a more aggressive phenotype, including increased growth rate to cultured human prostate and breast cancer cells (22, 23). Upregulation of FGF8b was also observed in multiple human cancers, such as prostate, breast, and ovary carcinomas (24–28). The above findings strongly suggest that FGF8, especially FGF8b, is the potential target for antibody-based cancer therapy.

FGF signaling is transduced through the formation of a complex of a growth factor, a proteoglycan, and a high-affinity FGF receptor (FGFR), which is a transmembrane tyrosine kinase receptor (29). Four different high-affinity receptors (FGFR1, FGFR2, FGFR3, and FGFR4) bind FGF ligands and display varying patterns of expression (reviewed in refs. 1, 24). Extracellular domains of FGFRs consist of three immunoglobulin-like loops (loop I, II, and III). Alternative mRNA splicing of loop III of FGFR1 to FGFR3 leads to distinct functional variants (IIIb and IIIc) that have different ligand-binding specificities and affinities. FGFR4 does not have alternative splicing but is most similar to an IIIc-like domain (1, 30, 31). Differential expression of IIIb and IIIc variants is very important for determining FGF signaling specificity. For example, the expression of FGFR2 isoforms of IIIb and IIIc is restricted to the cells of epithelial and mesenchymal lineage, respectively. In addition, exon switching from FGFR2IIIb to FGFR2IIIc was observed in progressive prostate cancer (32). FGF8 preferentially activates FGFR2IIIc and FGFR3IIIc splice forms and FGFR4 (17, 33), although there are differences between the activation potential of various FGF8 isoforms. FGF8b also activates FGFR1IIIc but only at a very high concentration (17). The receptors are activated through dimerization and phosphorylation by the intracellular tyrosine kinase domains (34). This process activates the Ras signal transduction pathway via FGFR substrate 2 (FRS2), the key components of which are the mitogen-activated protein kinases (MAPK) extracellular signal-regulated kinase (ERK) 1 ($p44^{MAPK}$) and ERK2 ($p42^{MAPK}$; for reviews, see refs. 35, 36).

We had already established a neutralizing monoclonal anti-FGF8b antibody, KM1334, by immunizing FGF8b-derived peptide. KM1334 was shown to inhibit androgen- and FGF8b-dependent growth of SC-3 cells *in vitro* (24). Furthermore, high frequency of FGF8 expression in clinical prostate cancers and breast diseases was immunohistochemically shown by KM1334 (24, 26), which is consistent with the results of immunohistochemistry and *in situ* hybridization reported by other groups (25, 27).

To investigate the potential of KM1334 as therapeutic agent for the treatment of cancers that are dependent on FGF8b signaling for growth and survival, we further evaluated its binding specificity, blocking activity, and *in vivo* antitumor activity. We show that KM1334 possesses high specificity and potent blocking activity *in vitro*. In addition, we show that this antibody exhibit strong antitumor activity *in vivo* mice model and its activity is mediated by both antiproliferative and proapoptotic activities.

Materials and Methods

Antibodies. A murine mAb against FGF8b, KM1334, was established as described previously (24). Briefly, the keyhole limpet hemocyanin–conjugated FGF8b peptide (FGF8b-1) from amino acid residues 23 to 46 of human and mouse FGF8b was used as an immunogen. A murine mAb, KM511, raised against a mutant of granulocyte colony-stimulating factor was described previously (37) and used as a negative control.

Anti-phosphospecific ERK1/2 rabbit polyclonal antibody and anti-phosphorylated FRS2α rabbit polyclonal antibody were obtained from Cell Signaling Technology (Beverly, MA). Anti-ERK2 mAb (clone 1B3B9) and anti-FRS2 rabbit polyclonal antibody (H-91) was purchased from Upstate Biotechnology (Lake Placid, NY) and Santa Cruz Biotechnology (Santa Cruz, CA), respectively. Anti-β-actin mouse mAb (ab8226) was from Abcam (Cambridge, United Kingdom).

Cells and animals. The SC-3 cell line used in the present study was derived from an androgen-responsive mouse mammary SC115 tumor (38). Adult male BALB/c *nu/nu* mice were purchased from Nippon Clea Co. (Tokyo, Japan).

Synthesis of fibroblast growth factor 8 fragment. Peptides with amino acid residues from 23 to 35 of human FGF8a (FGF8a-1), from 23 to 46 of human FGF8b (FGF8b-1), from 23 to 64 of human FGF8e (FGF8e-1), and from 23 to 75 of human FGF8f (FGF8f-1) were synthesized by an automated peptide synthesizer. For inhibition ELISA, FGF8b fragment (FGF8b-1) with additional cysteine residue in COOH terminus was synthesized and conjugated to bovine serum albumin (BSA).

Cross-reactivity of KM1334 to human fibroblast growth factor 8 variants (inhibition ELISA). The FGF8b-1 peptide conjugated to BSA was plated onto 96-well plate at a concentration of 1.0 μg/mL per 50 μL of each well. After overnight plating at 4°C, the plate was washed with PBS and blocked with 1% BSA in PBS. Then, the synthetic peptides, FGF8a-1, FGF8b-1, FGF8e-1, FGF8f-1, and a control peptide with a irrespective sequence (CGAGPKRRALAAPAAEEKEEA), were serially diluted and added into each well with KM1334 (final concentration, 0.08 μg/mL). After 2 hours of incubation at room temperature, the plate was interacted with horseradish peroxidase–labeled anti-mouse immunoglobulins (DAKO Corp., Carpinteria, CA) and 2,2′-azino-bis(3-ethylbenz-thiazoline-6-sulfonic acid substances, WAKO, Osaka, Japan). The absorbance at 415 nm was measured using an E-max microplate reader (Molecular Devices Corp., Sunnyvale, CA).

Cross-reactivity of KM1334 to human fibroblast growth factor 17b and fibroblast growth factor 18 (binding ELISA). Recombinant human FGF17b (R&D Systems, Inc., Minneapolis, MN), human FGF18 (R&D Systems), mouse FGF8b (R&D Systems), and human FGF2 (PeproTech, London, United Kingdom) were plated onto 96-well plate at serial concentrations from 0.1 ng/mL to 10 μg/mL per 50 μL of each well. After overnight plating at 4°C, the plate was serially washed and blocked with 1% BSA, and KM1334 was added into each well at a concentration of 1 μg/mL per 50 μL of each well. After washing, the bound antibody was detected as described previously.

Binding activity of fibroblast growth factor receptor-Fc fusion proteins to fibroblast growth factor 8b (binding ELISA). FGFRs fused with human IgG1 Fc domain (FGFR-Fc fusion proteins; human FGFR1IIIc-Fc, human FGFR2IIIc-Fc, murine FGFR3IIIc-Fc, and human FGFR4-Fc) were

purchased from R&D Systems. Production of a negative control, human interleukin (IL)-5 receptor (IL-5R)-Fc fusion protein, will be described elsewhere.[4] FGF8b was coated onto 96-well plate at a concentration of 5 μg/mL. After washing, the wells were incubated with serial concentrations of the FGFR-Fc and IL-5R-Fc fusion proteins. Bound FGFR-Fc fusion proteins on FGF8b were detected with anti-human IgG labeled with horseradish peroxidase (American Qualex, San Clemente, CA) diluted 1:12,500 as a secondary antibody. Inhibition of the FGF8b binding to FGFR-Fc fusion proteins by KM1334 was evaluated in this system. Serially diluted KM1334 or KM511 were added with each FGFR-Fc solution (10 μg/mL FGFR2IIIc-Fc, 2 μg/mL FGFR3IIIc-Fc, and 1 μg/mL FGFR4-Fc) to the FGF8b-coated plate. After washing, the secondary antibody bound to human Fc was detected as described previously.

Western blot. SC-3 cells were plated into 10 cm dishes at 2×10^6 cells per dish in a serum-supplemented medium; 2S(−) [Ham's F-12:DMEM (1:1, v/v) containing 2% dextran-coated, charcoal-treated fetal bovine serum] and allowed to adhere. After 8 hours of incubation at 37°C, the medium was exchanged with a serum-free medium; B0.1 [Ham's F-12:DMEM (1:1, v/v) containing 2% BSA] and incubated for 16 hours. Then, the medium was changed to an experimental medium composed of B0.1 and incubated for 15 minutes. After wash with PBS, cells were lysed in 500 μL lysis buffer [50 mmol/L HEPES-NaOH (pH 7.4), 250 mmol/L NaCl, 1 mmol/L EDTA, 1% NP40, 1 mmol/L DTT, 1 mmol/L phenylmethylsulfonyl fluoride, 5 μg/mL leupeptin, 2 mmol/L Na_3VO_4, 1 mmol/L NaF, 10 mmol/L β-glycerophosphate; ref. 39]. Cell lysates were clarified by centrifugation and total cell lysate (20 μg) from each sample was used for SDS-PAGE. After SDS-PAGE, the protein were transferred to polyvinylidene difluoride membranes and immunoblotted with appropriate secondary antibodies conjugated with horseradish peroxidase and developed using the enhanced chemiluminescence detection system according to the instructions of the manufacturer (Amersham Pharmacia Biotech, Piscataway, NJ).

Immunocytochemistry for SC-3 cells. SC-3 cells were inoculated into eight-well chamber slides (Nalge Nunc International, Rochester, NY) at 1×10^4 cells per well suspended in 200 μL 2S(−) medium and allowed to adhere. After 16 hours of incubation at 37°C, the medium was changed to an experimental medium composed of B0.1 and incubated for 24 hours. After wash with PBS, the chambers were removed and the slides were air-dried for 24 hours. Then, the cells were fixed in a 1:1 mixture of acetone/methanol for 10 minutes at room temperature. The slides were immunocytochemically stained for incorporated 5-bromo-2′-deoxyuridine (BrdUrd; Sigma Chemical Co., St. Louis, MO) labeling and terminal deoxynucleotidyl transferase–mediated nick end labeling (TUNEL) method (40). For BrdUrd labeling, BrdUrd was added to the medium at 100 μmol/L concentration for 1 hour before PBS wash. Then, the slides were treated with 3% H_2O_2 and 2 N HCl. BrdUrd incorporated into SC-3 cells was detected with a mouse anti-BrdUrd antibody (DAKO A/S, Glostrup, Denmark), EnVision, and 3,3′-diaminobenzidine (Merck, Darmstadt, Germany). Mayer's hematoxylin (Muto Pure Chemicals Ltd., Tokyo, Japan) was used for counterstaining. Positive cells and total cells in the three independent areas of 370 × 500 μm were counted. TUNEL method was done using the ApopTag Apoptosis *In situ* Detection Kit (Intergen, Purchase, NY) according to the manufacturer's instruction. Briefly, the slides were treated with 3% H_2O_2 and the nick ends of DNA were labeled with digoxigenin by terminal deoxynucleotidyl transferase enzyme. Apoptotic cells were detected with an anti-digoxigenin peroxidase conjugate using 3,3′-diaminobenzidine (WAKO) as a substrate. Mayer's hematoxylin was used for counterstaining. Positive cells and total cells in the three independent areas of 370 × 500 μm were counted. Statistical significances in the ratio of BrdUrd- or TUNEL-positive cells between the KM1334 group and the KM511 group were determined by two-tailed unpaired *t* test.

Evaluation of antitumor activity. All of the *in vivo* experiments were done in conformity with institutional guidelines in compliance with national laws and policies. SC-3 cells were harvested, washed with PBS, and inoculated s.c. in the dorsal side of male athymic nude mice by 1×10^6 cells per head suspended with 100 μL PBS. Tumors were allowed to reach ~300 mm^3 in size, and the mice were randomized into groups of five animals each. Mice were treated with KM1334 (50, 100, 200, and 400 μg in 200 μL PBS/mouse/shot) or PBS (200 μL/mouse/shot) by i.p. injection twice weekly. Treatment of animals was continued for the duration of the study (total of nine shots). Tumors were measured twice weekly with calipers, and tumor volumes were calculated by the following formula according to the methods of the National Cancer Institute (ref. 41; length and width of the tumors measured in mm): Tumor volume (mm^3) = (Length × $Width^2$) / 2.

Statistical significances in tumor size between the KM1334 group and the vehicle control (PBS) group were determined by two-tailed unpaired *t* test.

Immunohistochemistry for tumor sections. SC-3 cells were inoculated into athymic male nude mice according to the method written above. When SC-3 tumors reached 120 to 600 mm^3 in size, the mice were randomized into seven groups of three animals each. KM1334 and KM511 were given into three groups each by 400 μg in 200 μL PBS/mouse/shot. Tumors were collected at timings as follows: before antibody injection and at 7, 24, and 72 hours after antibody injection. Tumor volume was also measured immediately before each collection of tumors. One hour before tumor collection, BrdUrd dissolved in saline (20 mg/mL) was given i.v. into the mice by 100 mg/kg. The collected tumors were cut into two aliquots and were fixed in 10% neutral buffered formalin, embedded in paraffin, and sectioned at 3 μm. After deparaffinization and rehydration, sections were immunohistochemically stained for incorporated BrdUrd labeling and TUNEL method as described in immunocytochemistry of SC-3 cells (40). For BrdUrd labeling, sections were treated with 0.05% Pronase after neutralization with sodium borate. For TUNEL staining, sections were treated with proteinase K (Life Technologies, Rockville, MD) before digoxigenin labeling with terminal deoxynucleotidyl transferase enzyme. Positive cells in the area of 320 × 420 μm were counted. Statistical significances in BrdUrd- or TUNEL-positive cells between the KM1334 group and the KM511 group were determined by two-tailed unpaired *t* test.

Results

Binding specificity of an anti–fibroblast growth factor 8b monoclonal antibody, KM1334. To evaluate the therapeutic potential of an anti-FGF8b mAb KM1334, we first analyzed its specificity. We generated four synthetic peptides derived from human FGF8 variants (a, b, e, and f) and examined their inhibitory effect on the binding of KM1334 to its epitope-containing conjugate (FGF8b-1-BSA conjugate) in ELISA. Figure 1A and B show the structure of human FGF8 protein isoforms and the amino acid sequences of the synthetic peptides. Among the peptides examined, FGF8b-1 and FGF8f-1 significantly inhibited the binding of KM1334 to its antigen, indicating that KM1334 recognizes both FGF8b and FGF8f isoforms (Fig. 1C). On the other hand, FGF8a-1 and FGF8e-1 did not inhibit the binding. The lack of binding of KM1334 to FGF8a-1 is consistent with previously reported results (24). We next examined the cross-reactivity of KM1334 to FGF17b and FGF18, which are the closest members of FGF8 in FGF family, and their sequences corresponding to FGF8b-1 have significant homology with FGF8b (Fig. 2A). KM1334 showed strong binding to FGF8b; however, KM1334 did not bind to FGF17b,

[4] M. Koike et al. Anti-human IL-5Rα neutralizing monoclonal antibodies, manuscript in preparation.

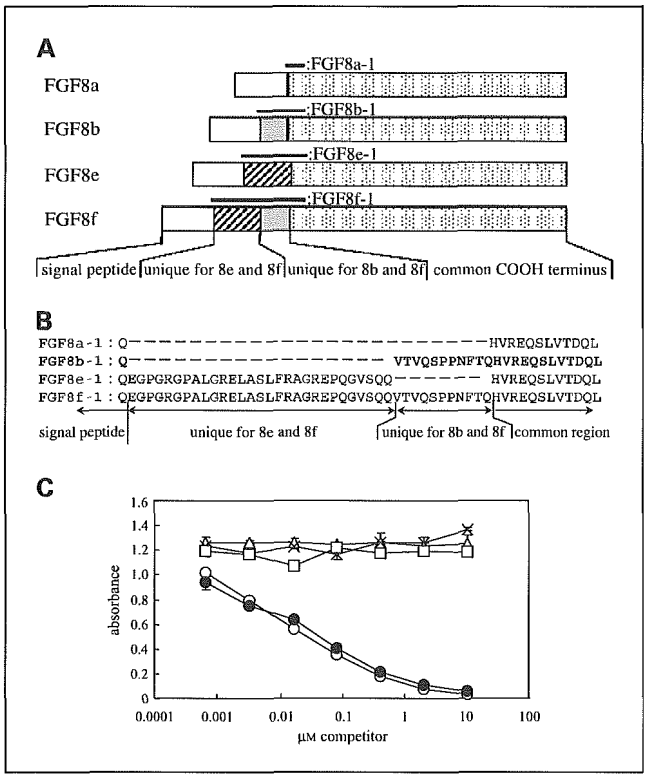

Fig. 1. Specificity of KM1334 to FGF8 variants. *A*, human premature FGF8a, FGF8b, FGF8e, and FGF8f protein isoforms, depicted NH_2 terminus (*left*) to COOH terminus (*right*). Solid bars above each columns, region used for synthetic peptides (*right*). *B*, alignment of amino acid sequences belonging to human FGF8 isoforms. FGF8a-1, FGF8b-1, FGF8e-1, and FGF8f-1 correspond to partial sequences of FGF8a, FGF8b, FGF8e, and FGF8f, respectively. KM1334 was raised against FGF8b-1 (*bold*) that includes unique sequence for FGF8b and FGF8f (VTVQSPPNFTQ). All four synthetic peptides were designed to contain the shared sequence (HVREQSLVTDQL) of all FGF8 isoforms. FGF8b-1 and FGF8f-1 contained unique sequence for FGF8b and FGF8f. FGF8e-1 and FGF8f-1 contained unique sequence for FGF8e and FGF8f. Gaps were introduced to facilitate understanding of the identity among each sequence. *C*, inhibition ELISA to analyze binding specificity of FGF8 variants: FGF8b-1 (○; positive control), FGF8f-1 (●), FGF8a-1 (△), FGF8e-1 (×), and peptide for negative control (□). Points, mean for $A_{415\text{-}490}$; bars, SD.

FGF18, and FGF2 (Fig. 2B). These results show that KM1334 possesses the high specificity to FGF8b.

Neutralizing activity of KM1334. Since Tanaka et al. reported that KM1334 inhibited SC-3 growth *in vitro* (24), direct evidence of blocking activity of KM1334 has not been shown yet. We first examined the binding of FGF8b to FGFR-Fc fusion proteins (FGFR1IIIc-Fc, FGFR2IIIc-Fc, FGFR3IIIc-Fc, and FGFR4-Fc) in ELISA. Among FGFR-Fc fusion proteins tested, FGFR2IIIc-Fc, FGFR3IIIc-Fc, and FGFR4-Fc showed significant binding activity to FGF8b; however, FGFR1IIIc-Fc showed little binding to FGF8b (Fig. 3A). The order of affinity was as follows: FGFR4-Fc ≧ FGFR3IIIc-Fc > FGFR2IIIc-Fc. The apparent affinities of FGFR4-Fc and FGFR3IIIc-Fc with FGF8b were 32.2- and 11.3-fold higher than that of FGFR2IIIc-Fc, respectively. Then, the ability of KM1334 to block the FGF8b binding to FGFR-Fc fusion proteins was assessed in this ELISA. KM1334 blocked the binding of FGF8b to all the FGFR-Fc fusion proteins examined: FGFR2IIIc-Fc (IC_{50}, 0.31 μg/mL; Fig. 3B), FGFR3IIIc-Fc (IC_{50}, 0.86 μg/mL; Fig. 3C), and FGFR4-Fc (IC_{50}, 0.95 μg/mL; Fig. 3D). Control antibody KM511 did not show any blocking activity.

To identify FGF8b-stimulated signal transduction pathway in SC-3 cells, phosphorylation of FRS2α and MAPK (ERK1/2) was examined in Western analysis. Phosphospecific antibodies against FRS2α and ERK1/2 gave stronger signal to FGF8b-stimulated cells than nonstimulated control cells. The expression level of ERK2 was almost the same in all samples (Fig. 4A). On the other hand, FRS2 expression seemed to be up-regulated slightly in the FGF8-stimulated cells. KM1334 inhibited FGF8b-induced phosphorylation of both FRS2α and ERK1/2 in a dose-dependent manner (Fig. 4A).

Furthermore, immunocytochemical analysis revealed that FGF8b promotes uptake of BrdUrd and rescues apoptosis in SC-3 cells, which show that FGF8b is critical for the growth and survival of SC-3 cells. KM1334 also inhibited those effects in a dose-dependent manner (Fig. 4B and C), which was in agreement with a previous report demonstrating that KM1334 inhibited FGF8b- and androgen-dependent growth of SC-3 cells (24). These results indicate that KM1334 possesses the potent *in vitro* neutralizing activity.

In vivo *effect of KM1334 on SC-3 tumors in mice.* We next examined the potential of antitumor activity of KM1334 on the growth of SC-3 tumor implanted on nude mice. SC-3 cells were injected into male nude mice s.c. and allowed to grow to ~300 mm^3 in size. Antibody treatment of 50, 100, 200, and 400 μg/injection was started 10 days after tumor inoculation and the tumor sizes were monitored until day 38. As shown in Fig. 5, treatment with KM1334 resulted in dose-dependent suppression of SC-3 tumor growth. On day 38, at the end of the experiment, the treated versus control values (i.e., relative volume of treated tumors divided by the relative volume of control tumors × 100) of 50, 100, 200, and 400 μg treated groups were 60%, 53%, 19%, and 4.3%, respectively. Rapid regression of SC-3 tumors were observed in the maximum dose group of KM1334 (400 μg/injection).

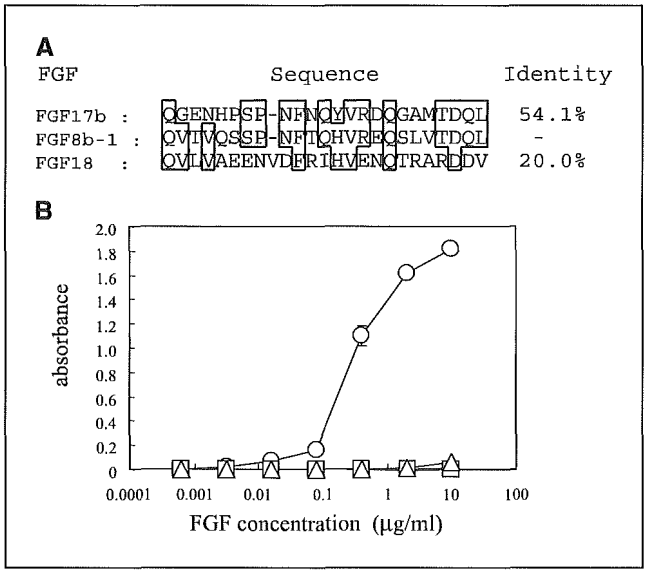

Fig. 2. Specificity of KM1334 to other members of FGF family with high homology to FGF8. *A*, alignment of amino acid sequences of FGF17b and FGF18 with FGF8b. Gaps were introduced to optimize the homology. Boxed area, shared residues in more than two FGFs. *B*, binding ELISA to detect cross-reactivity of KM1334 to other FGFs. A ELISA plate was coated for FGFs [i.e., FGF8b (○), basic-FGF (◆; negative control), FGF17b (△), and FGF18 (□)] at various concentrations and KM1334 was reacted to them at 1.0 μg/mL. Points, mean for $A_{415\text{-}490}$; bars, SD.

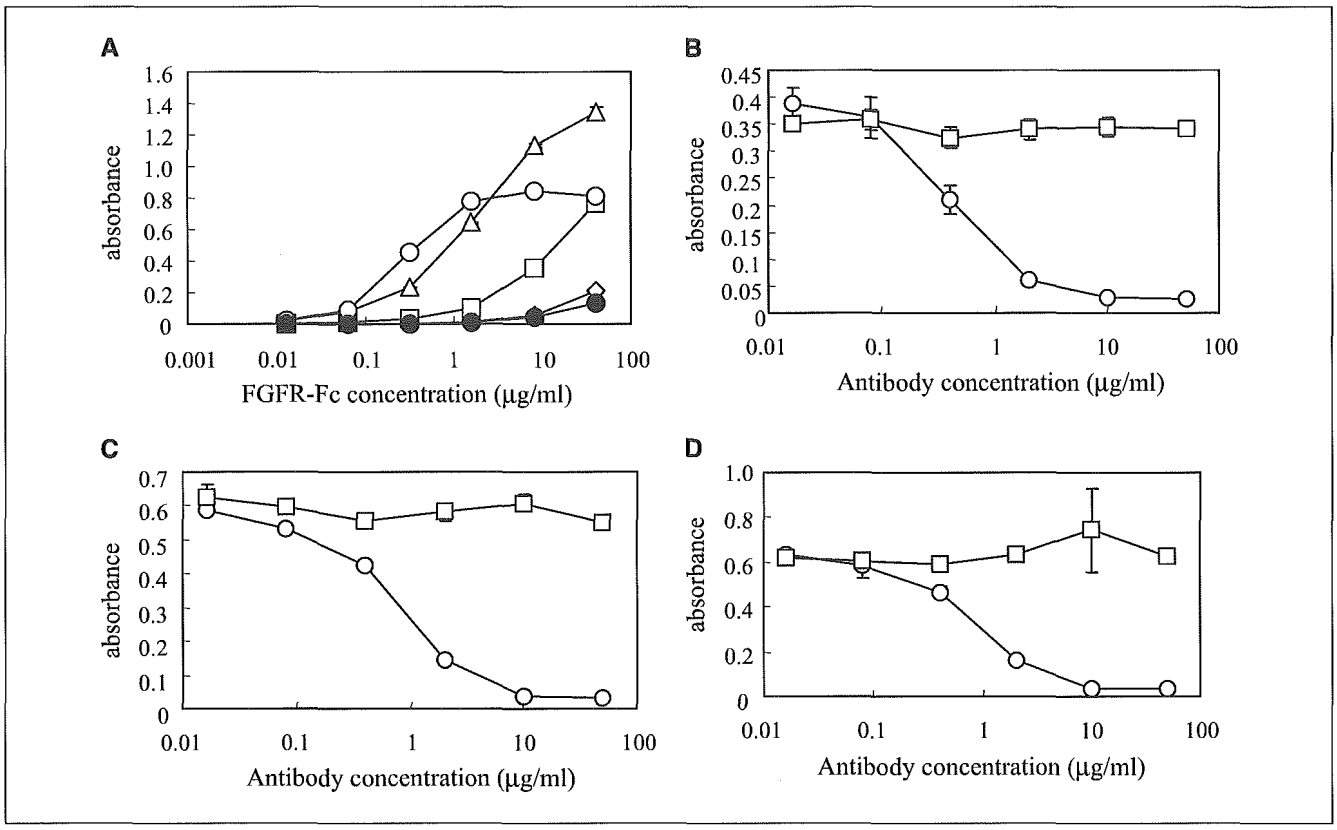

Fig. 3. Binding activity of FGFRs to FGF8b and their inhibition by KM1334. *A*, FGF8b was coated to a ELISA plate at concentration of 5 μg/mL. Then, FGFR extracellular domains fused to human Fc region [FGFR1IIIc-Fc (◇), FGFR2IIIc (□), FGFR3IIIc (△), and FGFR4 (○)] were reacted to the FGF8b at various concentrations. IL5R-human Fc fusion protein was used as a negative control (●). *B-D*, effect of KM1334 (○) and KM511 (□), negative control, on the binding of FGF8b to FGFR-Fc fusion proteins [FGFR2IIIc-Fc (*B*), FGFR3IIIc-Fc (*C*), and FGFR4-Fc (*D*)]. Points, mean for $A_{415\text{-}490}$; bars, SD.

To understand the mechanism by which tumors treated by 400 μg KM1334 regressed rapidly *in vivo*, histologic analysis was done on tumor sections from SC-3 tumor model, and tumor sections were stained for markers of cell proliferation and apoptosis. Figure 6A shows the effect of KM1334 on cumulative BrdUrd incorporation at three time points (7, 24, and 72 hours). Twenty-four hours after treatment with KM1334, there was a remarkable reduction in BrdUrd incorporation persisting until 72 hours, which is suggestive of arrest in G_0-G_1. We next examined the effect of KM1334 on apoptosis over the same time course via TUNEL labeling (Fig. 6B). The number of apoptotic cells increased markedly between 7 and 24 hours and decreased to the level of control by 72 hours. These results suggested that inhibition of cell proliferation and induction of apoptosis were responsible for the dramatic regression of tumor size *in vivo*.

Discussion

To our knowledge, this is the first report that describes mAb against FGF8 for therapeutic use. We showed that an anti-FGF8b murine mAb, KM1334, suppressed SC-3 tumor growth dose-dependently and the maximum dose injection of the antibody caused rapid regression of SC-3 tumors established in nude mice accompanied by inhibition of cell proliferation and induction of apoptosis. KM1334 showed very high specificity to FGF8b and FGF8f out of FGF family members examined and potent blocking activity of FGF8b binding to its three receptors (FGFR2IIIc, FGFR3IIIc, and FGFR4) and FGF8b-induced downstream signaling. These results provide the rationale for further development of KM1334 as a candidate anticancer therapeutic agent against FGF8b-dependent tumors.

Contribution of FGFs, including FGF2, FGF5, FGF8, etc., as autocrine and/or paracrine growth factors in tumorigenesis have been widely studied (31, 42); however, there are only limited reports that showed the potential of anti-FGF ligand neutralizing antibodies as candidates of therapeutic agents. Although several groups reported that anti-FGF2 antibodies showed antitumor activities *in vivo* (43, 44), they were not so potent as observed in this study. We show for the first time that FGF ligands are very potent targets for antibody-based cancer therapy.

Many studies reported up-regulation of FGF8 in various clinical cancers, including prostate and breast cancers, and the strongest mitogenic isoform FGF8b among human FGF8 variants (a, b, e, and f) is considered to be the most important for the progression of those diseases (22, 23, 25, 27). FGF8f has the second strongest mitogenic activity in human FGF8 isoforms (17, 31) and coexpression of FGF8f with FGF8b resulted in worse prognosis than single expression of FGF8b in esophageal carcinoma (45). Therefore, inhibition of both FGF8b and FGF8f activity might be desirable for the therapy

of FGF8-associated cancers. It was already shown that KM1334 specifically recognizes FGF8b among murine FGF8 variants (a-c); however, it was unclear which human FGF8 variants KM1334 recognizes. Among synthetic peptides derived from four human

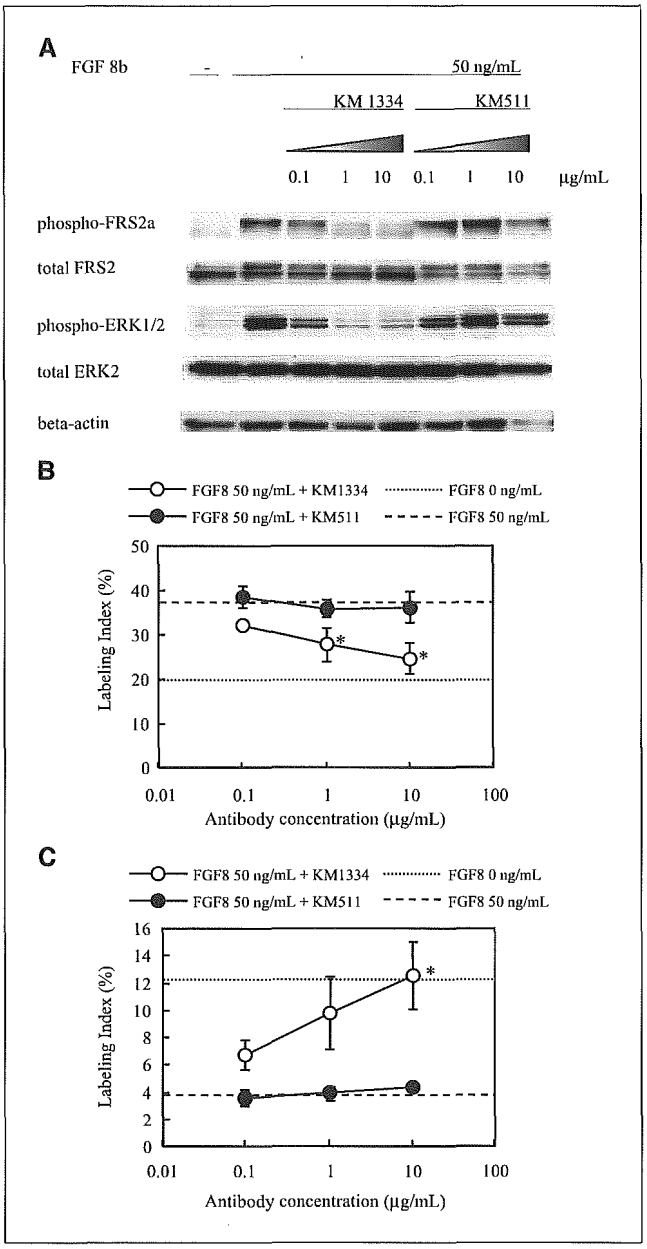

Fig. 4. *In vitro* effect of KM1334 on SC-3 cells stimulated by FGF8b. *A*, Western blot analysis. SC-3 cells were stimulated by 50 ng/mL FGF8b with KM1334 or KM511 (isotype control). After 15 minutes of incubation at 37°C, cells were collected and cell lysates were prepared. Western blot analyses were done using the indicated phosphospecific antibodies to FRS2α (Tyr^{196}) or ERK1/2 (Thy^{202}/Tyr^{204}), and the blots were reprobed with antibodies to total FRS2 or total ERK2. A representative β-actin reprobed blot is shown as a loading control. *B* and *C*, immunocytochemical analysis of SC-3 cells. SC-3 cells were stimulated by 50 ng/mL FGF8b with KM1334 or KM511. After 24 hours of incubation, BrdUrd was added and incubated for additional 1 hour. Uptake of BrdUrd was examined by anti-BrdUrd antibody with an immunocytochemical method (*B*). Results of TUNEL staining were shown in (*C*). Labeling index shows the number of 3,3′-diaminobenzidine-positive cells divided by the total number of nuclear pixels (hematoxylin-positive cells + 3,3′-diaminobenzidine-positive cells) multiplied by 100. Points, mean for three independent areas of 370 × 500 μm; bars, SD. Statistics were done by two-tailed Student's *t* test. *, $P < 0.05$, relative to control (*B* and *C*).

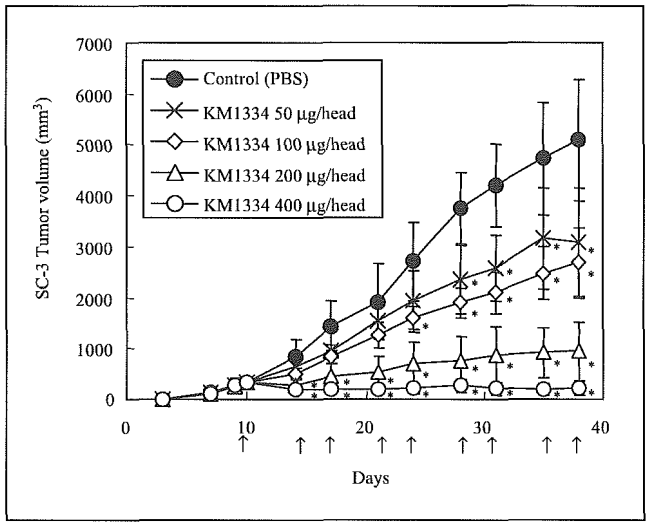

Fig. 5. Antitumor activity of KM1334 against SC-3 tumors established on nude mice. SC-3 cells were transplanted s.c. into adult male nude mice. SC-3 tumors were allowed to grow ~ 300 mm^3; then, KM1334 [50 μg/head (×), 100 μg/head (◇), 200 μg/head (△), or 400 μg/head (○)] and PBS (●), a vehicle control, were given into the mice twice weekly (total of nine times). Tumor volume was measured until day 38. Arrows below the transverse axis, days for antibody treatment. Points, mean for tumor volume ($n = 5$ each group); bars, SD. *, $P < 0.01$, relative to control, two-tailed Student's *t* test.

FGF8 variants, FGF8b-1 (derived from FGF8b and used for the immunogen of KM1334) and FGF8f-1 (derived from FGF8f) were proven to inhibit the binding of KM1334 to its antigen, indicating that KM1334 recognize both FGF8b and FGF8f isoforms (Fig. 1C). Human FGF17 and FGF18 have been isolated recently and form a subfamily with FGF8 in FGFs. Their amino acid sequences corresponding to FGF8b-1 have significant identity to FGF8b (FGF17, 54.1%; FGF18, 20.0%; Fig. 2A); however, KM1334 did not bind to FGF17b and FGF18 (Fig. 2B). These results indicate that KM1334 possesses high specificity enough to target FGF8b and FGF8f selectively.

Although colocalization of FGF8 and its receptors was identified in various neoplastic tissues (27, 28, 45), it was still unknown which type of FGFRs are activated by FGF8. Therefore, an anti-FGF8 neutralizing mAb, which has the ability to inhibit FGF8-induced activation via all possible FGFRs, is desired. Relative mitogenic activities of FGF8 isoforms to each FGFR have already been described (17, 33); however, direct comparison of mitogenic activity or binding activity of FGF8b to FGFRs has never been reported. In this study, we could establish for the first time the ELISA system to detect direct binding of FGF8b to FGFR-Fc fusion proteins. In this system, FGFR4-Fc showed the most sensitive detection limit; however, FGFR3IIIc-Fc gave the highest value of the absorbance indicative of binding activity (Fig. 3A). The affinity of FGFR2IIIc-Fc to FGF8b was lower than that of FGFR3IIIc-Fc and FGFR4-Fc. These results were consistent with previous reports (17, 33). KM1334 inhibited the binding of FGF8b to all FGF8b receptors examined (FGFR2IIIc-Fc, FGFR3IIIc-Fc, and FGFR4-Fc) completely in the ELISA (Fig. 3B-D), which indicates that KM1334 has an ideal character as an inhibitor of FGF8b. It has already been shown that FGF8b-dependent growth of SC-3 cells is mediated by FGFR1IIIc (14, 46). However, in this study, the specific binding of FGFR1IIIc-Fc to FGF8b was not detected in the ELISA. Several

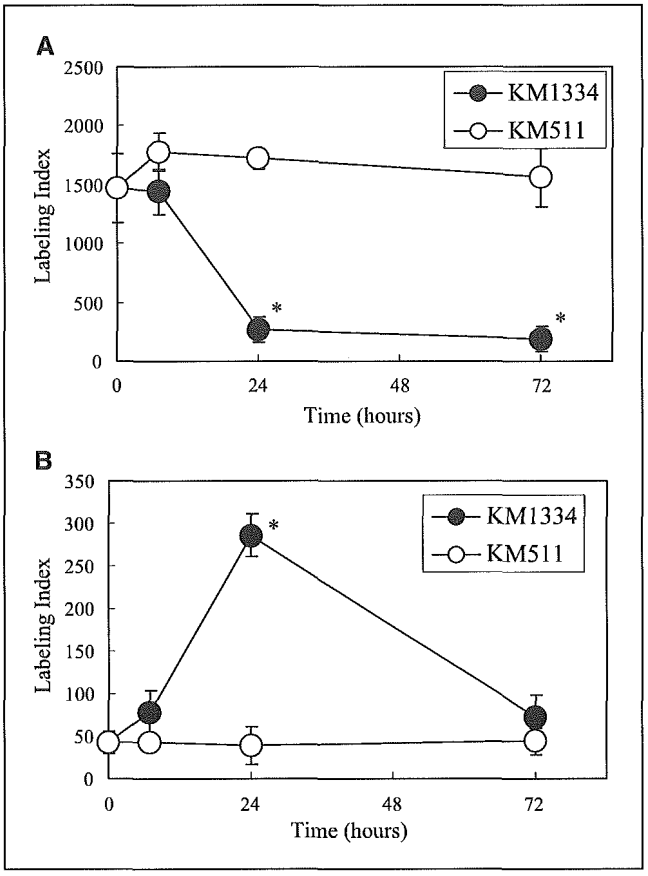

Fig. 6. Histologic analysis of SC-3 tumors treated with KM1334. *A*, uptake of BrdUrd. Mice carrying SC-3 tumors were treated with KM1334 (●) or KM511 (○), negative control. SC-3 tumors were collected before and at 7, 24, and 72 hours after antibody injection. Uptake of the BrdUrd was detected by anti-BrdUrd antibody. *B*, TUNEL staining. The same sample used for the BrdUrd uptake experiment was used for TUNEL staining. Labeling index indicates the number of 3,3′-diaminobenzidine-positive cells per mm^2. Points, mean for three independent areas; bars, SD. *, $P < 0.05$, relative to control, two-tailed Student's *t* test (*A* and *B*).

explanations of this discrepancy were possible. One explanation is that mutations in FGFR1IIIc (47) facilitate the binding between FGFR1IIIc and FGF8b in SC-3 cells. Another explanation, which is considered as more likely than the preceding one, is that concentration of FGF8b has significant effects on the detection of FGFR1IIIc-FGF8b binding. In previous reports, FGF8b could activate FGFR2IIIc, FGFR3IIIc, and FGFR4 at nanomolar concentrations (17, 33). However, FGFR1IIIc needs micromolar range of FGF8b concentration for its activation (17). Therefore, the binding between FGFR1IIIc and FGF8b in the ELISA might be enhanced by increasing the amount of FGF8b coated on the ELISA plate.

FRS2α is essential for the FGF-induced MAPK response (48) and ERK is a member of the MAPK implicated in the regulation of cell proliferation and differentiation. FGF8b treatment with SC-3 cells induced phosphorylation of both FRS2α and ERK1/2 (Fig. 4A), indicating that the FGF8b-induced proliferation of SC-3 cells is mediated by FGFR(s)-FRS2α-ERK1/2 signal transduction pathway. Together with the fact that KM1334 blocked this FGF8b-induced phosphorylation of FRS2α and ERK1/2 in SC-3 cells (Fig. 4A), FGF8b-neutralizing activity of KM1334 on SC-3 cell growth could be explained by the inhibition of FGF8b binding to its receptors and subsequent blockade of FGFR-mediated signal transduction.

Regression of SC-3 tumors by KM1334 treatment was explained by inhibition of cell proliferation and induction of apoptosis (Fig. 6A and B), which were well consistent with *in vitro* results shown in Fig. 4B and C. Together with the fact that that the antitumor effect of KM1334 was equal to castration (data not shown), it was suggested that FGF8b is critical to the androgen-dependent growth of SC-3 cells *in vivo* as well as *in vitro*. These results indicate that KM1334 might become a good therapeutic reagent against FGF8b-dependent tumors. In clinical prostate carcinoma in which androgen ablation therapy was effective, increase of the apoptotic index and decrease of mitotic index of tumors were detected (49, 50). Although the period of treatment was different, the same phenomenon was observed in the regressing SC-3 tumors treated with KM1334 (Fig. 6). Because the expression of FGF8 was identified in hormone-refractory prostate cancer as well as in hormone-responsive cancer (15), KM1334 may also be effective against hormone-refractory prostate cancer. As additional supportive evidence of this possibility, we have recently shown that overexpression of FGF8b in human prostate cancer LNCaP cells gave growth advantage to the cells *in vitro* and *in vivo*, and KM1334 could inhibit tumor growth in xenograft models of FGF8b-transfected LNCaP cells under androgen-dependent and androgen-independent conditions.[5] Further analysis, including additional *in vivo* xenograft studies and future clinical studies, might be needed to fully address the importance and contribution of FGF8b in human cancers.

Because amino acid sequences of mouse and human FGF8b are 100% identical (16), KM1334 could block endogenous FGF8b in mice. Administration of KM1334 caused no apparent toxicity, like weight loss or death to mice (data not shown), suggesting that targeting FGF8b in adult human might not cause severe side effects, although further studies are needed to fully analyze the side effects.

[5] K. Maruyama-Takahashi et al. An anti–fibroblast growth factor (FGF) 8 monoclonal antibody, KM1334, inhibits the growth of FGF8b-overexpressing LNCaP xenografts under androgen-dependent and -independent conditions, submitted for publication.

References

1. Kohler G, Milstein C. Continuous cultures of fused cells secreting antibody of predefined specificity. Nature (London) 1975;256:495–7.
2. Brekke OH, Sandlie I. Therapeutic antibodies for human diseases at the dawn of the twenty-first century. Nat Rev Drug Discov 2003;2:52–62.
3. Hurwitz H, Fehrenbacher L, Novotny W, et al. Bevacizumab plus irinotecan, fluorouracil, and leucovorin for metastatic colorectal cancer. N Engl J Med 2004;350:2335–42.
4. Szebenyi G, Fallon JF. Fibroblast growth factors as multifunctional signaling factors. Int Rev Cytol 1999;185:45–106.
5. Draper BW, Stock DW, Kimmel CB. *Zebrafish fgf24* functions with *fgf8* to promote posterior mesodermal development. Development 2003;130:4639–54.
6. Tanaka A, Miyamoto K, Minamino N, et al. Cloning and characterization of an androgen-induced growth factor essential for the androgen-dependent growth of mouse mammary carcinoma cells. Proc Natl Acad Sci U S A 1992;89:8928–32.

7. Ohuchi H, Yoshioka H, Tanaka A, Kawakami Y, Nohno T, Noji S. Involvement of androgen-induced growth factor (FGF-8) gene in mouse embryogenesis and morphogenesis. Biochem Biophys Res Commun 1994;204:882–8.
8. Mahmood R, Bresnick J, Hornbruch A, et al. A role for FGF-8 in the initiation and maintenance of vertebrate limb bud outgrowth. Curr Biol 1995;5:797–806.
9. Crossley PH, Martin GR. The mouse Fgf8 gene encodes a family of polypeptides and is expressed in regions that direct outgrowth and patterning in the developing embryo. Development 1995;121:439–51.
10. Crossley PH, Minowada G, MacArthur CA, Martin GR. Roles for FGF8 in the induction, initiation, and maintenance of chick limb development. Cell 1996; 84:127–36.
11. Crossley PH, Martinez S, Martin GR. Midbrain development induced by fgf8 in the chick embryo. Nature 1996;380:66–8.
12. Heikinheimo M, Lawshe A, Shackleford GM, Wilson DB, MacArthur CA. Fgf-8 expression in the post-gastrulation mouse suggests roles in the development of the face, limbs and central nervous system. Mech Dev 1994;48:129–38.
13. Lewandoski M, Meyers EN, Martin GR. Analysis of Fgf8 gene function in vertebrate development. Cold Spring Harb Symp Quant Biol 1997;62:159–68.
14. Kouhara H, Koga M, Kasayama S, Tanaka A, Kishimoto T, Sato B. Transforming activity of a newly cloned androgen-induced growth factor. Oncogene 1994;9:455–62.
15. Dorkin TJ, Robinson MC, Marsh C, Bjartell A, Neal DE, Leung HY. FGF8 over-expression in prostate cancer is associated with decreased patient survival and persists in androgen independent disease. Oncogene 1999;18:2755–61.
16. Gemel J, Gorry M, Ehrlich GD, MacArthur CA. Structure and sequence of human FGF8. Genomics 1996;35:253–7.
17. MacArthur CA, Lawshe A, Xu J, et al. FGF-8 isoforms activate receptor splice forms that are expressed in mesenchymal regions of mouse development. Development 1995;121:3603–13.
18. MacArthur CA, Lawshe A, Shankar DB, Heikinheimo M, Shackleford GM. FGF-8 isoforms differ in NIH3T3 cell transforming potential. Cell Growth Differ 1995;6:817–25.
19. Ghosh AK, Shankar DB, Shackleford GM, et al. Molecular cloning and characterization of human FGF8 alternative messenger RNA forms. Cell Growth Differ 1996;7:1425–34.
20. Daphna-Iken D, Shankar DB, Lawshe A, Ornitz DM, Shackleford GM, MacArthur CA. MMTV-Fgf8 transgenic mice develop mammary and salivary gland neoplasia and ovarian stromal hyperplasia. Oncogene 1998;17:2711–7.
21. Song Z, Wu X, Powell WC, et al. Fibroblast growth factor 8 isoform B overexpression in prostate epithelium: a new mouse model for prostatic intraepithelial neoplasia. Cancer Res 2002;62:5096–105.
22. Song Z, Powell WC, Kasahara N, van Bokhoven A, Miller GJ, Roy-Burman P. The effect of fibroblast growth factor 8, isoform b, on the biology of prostate carcinoma cells and their interaction with stromal cells. Cancer Res 2000;60:6730–6.
23. Ruohola JK, Viitanen TP, Valve EM, et al. Enhanced invasion and tumor growth of fibroblast growth factor 8b-overexpressing MCF-7 human breast cancer cells. Cancer Res 2001;61:4229–37.
24. Tanaka A, Furuya A, Yamasaki M, et al. High frequency of fibroblast growth factor (FGF) 8 expression in clinical prostate cancers and breast tissues, immunohistochemically demonstrated by a newly established neutralizing antibody against FGF 8. Cancer Res 1998; 58:2053–6.
25. Gnanapragasam VJ, Robinson MC, Marsh C, Robson CN, Hamdy FC, Leung HY. FGF8 isoform b expression in human prostate cancer. Br J Cancer 2003;88:1432–8.
26. Tanaka A, Kamiakito T, Takayashiki N, Sakurai S, Saito K. Fibroblast growth factor 8 expression in breast carcinoma: associations with androgen receptor and prostate-specific antigen expressions. Virchows Arch 2002;441:380–4.
27. Marsh SK, Bansal GS, Zammit C, et al. Increased expression of fibroblast growth factor 8 in human breast cancer. Oncogene 1999;18:1053–60.
28. Valve E, Martikainen P, Seppanen J, et al. Expression of fibroblast growth factor (FGF)-8 isoforms and FGF receptors in human ovarian tumors. Int J Cancer 2000; 88:718–25.
29. McKeehan WL, Wang F, Kan M. The heparan sulfate-fibroblast growth factor family: diversity of structure and function. Prog Nucleic Acid Res Mol Biol 1998;59:135–76.
30. Ornitz DM, Xu J, Colvin JS, et al. Receptor specificity of the fibroblast growth factor family. J Biol Chem 1996;271:15292–7.
31. Powers CJ, McLeskey SW, Wellstein A. Fibroblast growth factors, their receptors and signaling. Endocr Relat Cancer 2000;7:165–97.
32. Yan G, Fukabori Y, McBride G, Nikolaropolous S, McKeehan WL. Exon switching and activation of stromal and embryonic fibroblast growth factor (FGF)-FGF receptor genes in prostate epithelial cells accompany stromal independence and malignancy. Mol Cell Biol 1993;13:4513.
33. Blunt AG, Lawshe A, Cunningham ML, Seto ML, Ornitz DM, MacArthur CA. Overlapping expression and redundant activation of mesenchymal fibroblast growth factor (FGF) receptors by alternatively spliced FGF-8 ligands. J Biol Chem 1997;272:3733–8.
34. Ullrich A, Schlessinger J. Signal transduction by receptors with tyrosine kinase activity. Cell 1990;61: 203–12.
35. Denhardt DT. Signal-transducing protein phosphorylation cascades mediated by Ras/Rho proteins in the mammalian cell: the potential for multiplex signalling. Biochem J 1996;318:729–47.
36. Klint P, Claesson-Welsh L. Signal transduction by fibroblast growth factor receptors. Front Biosci 1999;4: D165–77.
37. Yoshida H, Shitara S. Generation and characterization of monoclonal antibodies to recombinant human granulocyte-colony stimulating factor (G-CSF) and its muteins. Agric Biol Chem 1989;53:1095–101.
38. Yamanishi H, Nonomura N, Tanaka A, et al. Proliferation of Shionogi carcinoma 115 cells by glucocorticoid-induced autocrine heparin-binding growth factor(s) in serum-free medium. Cancer Res 1991;51:3006–10.
39. Soga S, Neckers LM, Schulte TW, et al. KF25706, a novel oxime derivative of radicicol, exhibits *in vivo* antitumor activity via selective depletion of Hsp90 binding signaling molecules. Cancer Res 1999;59: 2931–8.
40. Takaba K, Saeki K, Suzuki K, Wanibuchi H, Fukushima S. Significant overexpression of metallothionein and cyclin D1 and apoptosis in the early process of rat urinary bladder carcinogenesis induced by treatment with *N*-butyl-*N*-(4-hydroxybutyl)nitrosamine or sodium L-ascorbate. Carcinogenesis 2000; 21:691–700.
41. Geran RI, Greenberg NH, MacDonald MM, Schumacher AM, Abbott BJ. Protocols for screening chemical agents and natural products against animal tumors and other biological systems [part 3]. Cancer Chemother Rep 1972;3:1–103.
42. Moroni E, Dell'Era P, Rusnati M, Presta M. Fibroblast growth factors and their receptors in hematopoiesis and hematological tumors. J Hematother Stem Cell Res 2002;11:19–32.
43. Hori A, Sasada R, Matsutani E, et al. Suppression of solid tumor growth by immunoneutralizing monoclonal antibody against human basic fibroblast growth factor. Cancer Res 1991;51:6180–4.
44. Gross JL, Herblin WF, Dusak BA, et al. Effects of modulation of basic fibroblast growth factor on tumor growth *in vivo*. J Natl Cancer Inst 1993;85: 121–31.
45. Tanaka S, Ueo H, Mafune K, Mori M, Wands JR, Sugimachi K. A novel isoform of human fibroblast growth factor 8 is induced by androgens and associated with progression of esophageal carcinoma. Dig Dis Sci 2001;46:1016–21.
46. Sato B, Kouhara H, Koga M, et al. Androgen-induced growth factor and its receptor: demonstration of the androgen-induced autocrine loop in mouse mammary carcinoma cells. J Steroid Biochem Mol Biol 1993;47:91–8.
47. Kouhara H, Kasayama S, Saito H, Matsumoto K, Sato B. Expression cDNA cloning of fibroblast growth factor (FGF) receptor in mouse breast cancer cells: a variant form in FGF-responsive transformed cells. Biochem Biophys Res Commun 1991; 15:31–7.
48. Hadari YR, Gotoh N, Kouhara H, Lax I, Schlessinger J. Critical role for the docking-protein FRS2α in FGF receptor-mediated signal transduction pathways. Proc Natl Acad Sci U S A 2001;98:8578–83.
49. Szende B, Romics I, Torda I, Bely M, Szegedi Z, Lovasz S. Apoptosis, mitosis, p53, bcl(2), Ki-67 and clinical outcome in prostate carcinoma treated by androgen ablation. Urol Int 1999;63:115–9.
50. Szende B, Romics I, Minik K, et al. Repeated biopsies in evaluation of therapeutic effects in prostate carcinoma. Prostate 2001;49:93–100.

〈抄録〉第25回 日本臨床薬理学会年会 2004年9月17～18日 静岡
シンポジウム2（安全性分野）：トキシコゲノミクス―現状と臨床薬理学への応用―

4．日本人組織を用いたトキシコゲノミクス研究

大島康雄* 藤村昭夫*

我々の研究室では日本人由来の組織を用いたトキシコゲノミクス研究を行っている。現状では日本人組織を商業ベースで合法的に入手することはできないために、我々は自治医科大学附属病院で手術を受ける患者さんにご協力いただき、手術時に病変部位と同時にやむを得ず切除される正常組織を研究に利用することとした。動物実験で得られた情報だけではヒトへの外挿が必ずしも十分ではなく、ヒトで最終的に確認できればより好ましい。一方、臨床検体の入手には困難な点が多く、研究計画の自由度は低い。動物実験・細胞株を用いた研究と我々の様にヒト組織を用いた研究は相補的な位置づけとされ、それぞれの役割を担うことが期待される。

1．倫理評価ワーキンググループ：
治療を目的として我々の病院を訪れる患者さんから、研究のための組織を提供していただくにあたり、我々は倫理評価ワーキンググループを立ち上げ、研究計画の審査・インフォームドコンセント取得の手順・検体採取後の病理組織の評価・匿名化の手順・関係書類の保管などにつき詳細な検討を行った。倫理評価ワーキンググループの中には、宗教家・法律家などの学外委員も含まれている。彼らとの討論の中で、医療関係者以外の第三者から誤解を受けやすい点が一つ浮かび上がった。今回我々が研究に用いる検体は、従来の手術方法で切除されてしまう非病変部組織であり、通常廃棄処分される組織部分を研究へ利用させていただく計画であった。しかし、非医療関係者は、病変の治療のためには必要もないのに研究目的のためだけに正常組織を切除するものと誤解されるようであった。このような誤解を受けやすい部分を今後も啓発することによって、日本人組織を研究・開発に利用しやすい社会環境を形成してゆく必要がある。

2．臨床検体取得の現場：
患者さんよりインフォームドコンセントをいただき、附属病院の手術室から臨床検体を取得し、プライマリーカルチャーを作成することができた。我々が試みた範囲ではディスパーゼとトリプシンを併用する方法が安定した良好な結果をもたらすものと思われた[1]。得られた細胞は、上皮性の細胞として矛盾のない形態を示し、腎臓皮質由来の細胞の多くはGlut-2抗原及びγGTP活性を示し、尿細管由来であることが示された。また、肝臓由来の細胞はアルブミン産生能及びCyp3A4抗原の存在から、主に肝細胞であると判断した。

3．臨床検体を用いた遺伝子発現解析の問題点：
出版された論文とともに公開されたデータベース(http://www.ncbi.nlm.nih.gov/geo/)をレビューした結果、171の臨床検体を用いたGeneChipデータのうち29 Chip (17%)ではRNAの質が不良であると判定された。一方で63の非臨床検体を用いたGeneChipデータではRNAの質がすべて良と判定された。このようにすでに公開・出版されているデータですら臨床検体のデータには問題点があることが示された。これは、臨床検体の取り扱いの難しさを示している。同時に、臨床検体を用いた網羅的遺伝子発現解析の実行・データの解釈にはRNAの質に注意すべきであることも示している。
網羅的遺伝子発現解析のもう一つの問題点は、個別の遺伝子発現全てにつきそのデータの信頼性とそれが意味するところを研究者自身が検証しながら研究を進めていくことが困難であることがあげられる。このためチップデータ全体の質を管理することが必要と考えられる。我々が使用している

* 自治医科大学薬理学講座臨床薬理学部門
〒329-0498 栃木県河内郡南河内薬師寺 3311-1

Affymetrix 社の GeneChip システムでは、こうした実験の質の管理を行うために用いることのできる様々なパラメータを実験結果の一部として得ることができる。このようなパラメータにはバックグラウンドノイズ・ハウスキーピングジーンの 3'/5'比・パーセントプレゼントなどがある。こうしたパラメータを活用し、研究の質をコントロールしつつ臨床検体の処理・プライマリーカルチャーの作成を行うことによって、我々はより良質のプライマリーカルチャーを作成することができたと考えている。また、既知濃度のスパイク RNA を用いて検出系の定量性・ダイナミックレンジの検討も行った。その結果、1.5 pM~100 pM での範囲での RNA 濃度の読みとりの直線性は良好であった。

4. 日本人組織を用いる必要性～人種差の克服：

海外で調整済みのプライマリーカルチャーを用いることに比較して、日本人組織を用いた遺伝子発現解析の利点として、理論的には研究結果について人種差を懸念する必要がないこと、海外調整済みのプライマリーカルチャーの利用にかかわる資金や場合によっては知的所有権などが海外へ流出する心配がないこと等がある。もちろんヒト組織であるから、種差も存在しない。さらに、自前でヒト組織を調整するため、組織の質を制御することが可能である。

我々の研究室ではこれまでのところ 11 名分の組織を研究に使用している。この 11 名につきそれぞれ 3 回、薬物等の刺激に未曝露の状態で発現解析を行ったところ、約 44,000 のトランスクリプトの内、統計学的に有意に個人差がある（t-test p 値が 0.01 未満）トランスクリプトは 100 に満たなかった。大多数の遺伝子発現は、薬物未曝露の状態では有意な個人差が見られないと判断された。

5. 現状と限界：

これまで 20 以上の薬物をプライマリーカルチャーへ曝露し、遺伝子発現解析を行った。腎障害をしばしば起こすことによって臨床的に問題になる薬物を用いて、有意に誘導や抑制される遺伝子を同定した。現在その遺伝子発現の確認を進めるとともに、その細胞内での働きを解析している。また、クラスタリングされた遺伝子群に有意に高頻度に出現する転写因子（DNA binding protein）認識配列を検索するシステムを構築した。[2]

本稿で記載した、個人差の研究により得られた情報は、重要な基礎的検討である。先行している実験動物や培養細胞株の研究に追従する形で曝露化合物の数を増加することよりも、データの質を管理するプロセスや、未刺激の日本人プライマリー腎細胞にどのような遺伝子に個人差があるのかを明らかにすることは、日本人の臨床検体を取り扱っている我々が取るべき、より優先順位の高い課題である。これらこそが限られたリソースと与えられた条件のなかで今後の日本人組織を用いた研究を活かし、示唆に富む情報を提供するもである。

[1] Yasuo Oshima, Shinsuke Kurokawa, Akihiko Tokue, Hiroyuki Mano, Ken Saito, Makoto Suzuki, Masashi Imai, and Akio Fujimura. Primary Cell Preparation of Human Renal Tubluar Cells for Transcriptome Analysis. *Toxicology Mechanisms and Methods*, 14:309-316, 2004

[2] Yasuo Oshima, Yusuke Ishida, Ayumi Shinohara, Hiroyuki Mano, Akio Fujimura. Expression Profiling of Gene with Upstream Aml1 Recognition Sequence in Hematopoietic Stem Cell-Like Fractions from Individuals with the M2 Subtype of Human Acute Myeloid Leukemia. Annual Meeting for International Society of Experimental Hematology, New Orleans, LA. USA. Jul 16-20, 2004